Journal of Power Sources 196 (2011) 5053–5063

Contents lists available at ScienceDirect

Journal of Power Sources

journal homepage: www.elsevier.com/locate/jpowsour

A semi-empirical model for efficiency evaluation of a direct methanol fuel cell

Yu-Jen Chiu [a,*], T. Leon Yu [b], Ya-Chien Chung [a]

[a] Department of Mechanical Engineering, Technology and Science Institute of Northern Taiwan, Taipei 11202, Taiwan
[b] Department of Chemical Engineering & Materials Science, Fuel Cell Center, Yuan Ze University, Chung-Li, Taoyuan 32003, Taiwan

ARTICLE INFO

Article history:
Received 24 November 2010
Received in revised form 27 January 2011
Accepted 27 January 2011
Available online 2 February 2011

Keywords:
Direct methanol fuel cell
Efficiency
Model

ABSTRACT

Energy density and power density are two of the most significant performance indices of a fuel cell system. Both the indices are closely related to the operating conditions. Energy density, which can be derived from fuel cell efficiency, is especially important to small and portable applications. Generally speaking, power density can be easily obtained by acquiring the voltage and current density of an operating fuel cell. However, for a direct methanol fuel cell (DMFC), it is much more difficult to evaluate its efficiency due to fuel crossover and the complex architecture of fuel circulation. The present paper proposes a semi-empirical model for the efficiency evaluation of a DMFC under various operating conditions. The power density and the efficiency of a DMFC are depicted by explicit functions of operating temperature, fuel concentration and current density. It provides a good prediction and a clear insight into the relationship between the aforementioned performance indices and operating variables. Therefore, information including power density, efficiency, as well as remaining run-time about the status of an operating DMFC can be in situ evaluated and predicted. The resulting model can also serve as an important basis for developing real-time control strategies of a DMFC system.

1. Introduction

Energy density and power density are two of the most significant specifications of a fuel cell system. These performance indices usually correlate with commercial benefits of the products [1,2]. Generally speaking, power density can be easily obtained by acquiring the voltage and current density of an operating fuel cell. However, for a DMFC, it can be much more complex to evaluate its energy density or alternatively its efficiency. The real efficiency of a fuel cell is always less than the reversible thermodynamic efficiency due to voltage losses and fuel utilization losses. When hydrogen fuel is considered, the efficiency of a fuel cell can be evaluated simply based on its operating voltage, generated current and the flow rate of fuel [3]. An overabundance of fuel supplying to a fuel cell without fuel recycling can lead to a waste. Nonetheless, for a DMFC, the architecture of fuel circulation is quite complicated, which makes difficulties in evaluating fuel utilization losses. Fuel crossover is one of the issues reducing the voltage efficiency and the fuel utilization efficiency of a DMFC [4]. To suppress the fuel crossover, the fuel concentration of a DMFC should be appropriately regulated between 1.5 M and 2.0 M to achieve optimum fuel cell efficiency [5]. Taking the energy density into account, fuel of higher concentration is usually stored in a fuel cell system. The fuel is then diluted in a mixing reservoir before being delivered into the fuel cell stack. The residual (unreacted) liquid fuel flowing through the anode is circulated back to the mixing reservoir and then to the stack again. Accordingly, the fuel utilization efficiency cannot be estimated merely by the generated current and the fuel flow rate. It is therefore essential to determine the amount of fuel crossover losses in a fuel cell stack.

The efficiency of a fuel cell is closely related to its operating conditions such as fuel concentration, operating temperature, current density (or operating voltage), rates of fuel delivered, etc. Jiang et al. proposed a method of fuel circulation with a fixed amount of fuel to investigate the efficiency of a DMFC under various operating temperatures [6]. Moreover, the influences of the initial fuel concentration and the operating temperature on the operating voltage of a passive (without fuel and air circulation) DMFC were also studied [7]. Liu et al. investigated the effect of the membrane thickness on the efficiency of a passive DMFC under various operating conditions [8]. Seo and Lee experimentally determined the methanol crossover fluxes and the efficiency of a DMFC where the cell temperature, methanol concentration, aqueous fuel flow rate, air flow rate and cathode backpressure were considered [9]. The aforementioned articles were mainly based on experimental approaches. Although these experimental approaches were straightforward, it was time-consuming and rather difficult to depict a whole picture of the efficiency under various operating conditions.

On the other hand, theoretical models are much more exact and can describe details and provide thorough information concerning the system [10–12]. Most of them are capable of forming a firm

* Corresponding author. Tel.: +886 2 28927154x8011; fax: +886 2 28935295.
E-mail address: yjchiu@tsint.edu.tw (Y.-J. Chiu).

0378-7753/$ – see front matter © 2011 Elsevier B.V. All rights reserved.
doi:10.1016/j.jpowsour.2011.01.084

Nomenclature

List of symbols

c	bulk methanol concentration in the channel ($mol\,cm^{-3}$)
D_A	effective diffusivity of methanol in anode catalyst layer ($cm^2\,s^{-1}$)
D_B	effective diffusivity of methanol in anode backing layer ($cm^2\,s^{-1}$)
D_m	effective diffusivity of methanol in membrane ($cm^2\,s^{-1}$)
E_r	thermodynamically reversible voltage (V)
F	Faraday's constant ($C\,mol^{-1}$)
Δg_{rxn}	the change of the Gibbs free energy of the reaction ($J\,mol^{-1}$)
Δh_{rxn}	the change of the enthalpy of the reaction ($J\,mol^{-1}$)
j	current density ($A\,cm^{-2}$)
K_1	partition coefficient at the interface between anode backing layer and anode catalyst layer
K_2	partition coefficient at the interface between anode catalyst layer and membrane
$\dot{N}_{eff}$	molar flux of the effective fuel consumption ($mol\,cm^{-2}\,s^{-1}$)
$\dot{N}_{mcr}$	methanol crossover flux ($mol\,cm^{-2}\,s^{-1}$)
n_d	electro-osmotic drag coefficient of water
n_f	remaining amounts of the fuel (mol)
p_{dmfc}	power density of a direct methanol fuel cell ($W\,cm^{-2}$)
R_e	area-specific resistance ($\Omega\,cm^2$)
T	temperature (K)
t_r	remaining run-time (h)
$\tilde{t}_r$	specific remaining run-time ($h\,cm^2\,mol^{-1}$)
V	operating fuel cell voltage (V)
δ_A	thickness of anode catalyst layer (cm)
δ_B	thickness of anode backing layer (cm)
δ_m	thickness of membrane (cm)
ε_{dmfc}	efficiency of a direct methanol fuel cell
ε_{fuel}	fuel utilization efficiency
ε_{thermo}	reversible thermodynamic efficiency
$\varepsilon_{voltage}$	voltage efficiency
λ	water content in Nafion
σ	ionic conductivity of membrane ($\Omega\,cm^2$)

basis to investigate the efficiency of a DMFC. Nonetheless, they are inevitably complex and require obscure numerical schemes for the solutions. Besides, parameters of the model should be measured or identified beforehand. Such a task is usually not easy; meanwhile, further experimental validation is essential. Due to the complexities of the solution process, theoretical models may be less practical for real-time applications. Accordingly, semi-empirical approaches are anticipated to correlate the experimental studies with the theoretical models that can serve as the basis for developing control strategies of a fuel cell system.

Since the voltage losses and the fuel utilization losses are the most significant factors determining the efficiency of a DMFC, we briefly review the polarization and the fuel crossover semi-empirical models. The semi-empirical models for the polarization behavior of a DMFC had been extensively investigated. Srinivasan et al. launched the issue by employing activation and ohmic losses to depict the polarization curves of a polymer electrolyte membrane fuel cell (PEMFC) [13]. Kim et al. then introduced an additional exponential term to govern the mass transport phenomenon and had a better fit to experimental results [14]. The mass transport term was modified by Squadrito et al. to provide a limit to the available current density [15]. Moreover, Kim's model was also modified and validated on a 30-cell stack by Chu and Jiang in which the physical meaning of the parameters was further discussed [16]. Because the mass transport limitations of a DMFC predominantly occur at the anode which differ from the case of a hydrogen fuel cell, Scott et al. studied the effects of methanol concentration on the anode polarization, together with an empirical open circuit voltage model and a cathode overpotential model, to predict the overall cell voltage [17]. Scott's group then introduced Kim's and Squadrito's models to a DMFC [18]. It revealed that Squadrito's model fitted the results better when the methanol concentration was lower than 0.75 M. Furthermore, a simple equation based on Squadrito's model was proposed and discussed by Scott's group [19]. To elucidate the effect of methanol crossover on a DMFC, O'Hayre et al. introduced an additional term to Scott's model to describe voltage losses due to current leakage and fuel crossover [3]. Tu et al. proposed a more complicated semi-empirical model for distinguishing the individual voltage losses due to methanol crossover and the cathode and anode overpotentials [20]. All the aforementioned semi-empirical models incorporated certain parameters whose values could be influenced by operating variables like temperatures and fuel concentrations. However, those parameters had not been expressed as functions of operating variables in the fitting procedures. Therefore, they are not suitable for predicting polarization behavior within a multi-dimensional domain of various operating variables.

The other essentiality of the efficiency model is the evaluation of fuel crossover. Semi-empirical models for evaluating methanol crossover fluxes had been extensively discussed [21–24]. In our previous work, a methanol crossover model was established analytically using an algebraic function in which fuel concentration, current density and operating temperature of a DMFC were considered [25]. It provides a good prediction and a clear picture of the methanol crossover behavior in a three-dimensional domain of operating variables. Consequently, the model is employed in this study for efficiency evaluation.

The major objective of this work is aimed at the efficiency evaluation of a DMFC in a multi-dimensional domain of various operating variables. The proposed semi-empirical model takes performance indices (i.e. power density and efficiency) and operating variables (i.e. fuel concentration, current density and temperature of the fuel cell) into a whole picture simultaneously. In the model, both the power density and the efficiency are stated in analytical functions which explicitly incorporate fuel concentration, current density and temperature of the fuel cell. Once the corresponding parameters of the model are determined, the quantitative prediction of power density and efficiency can be easily obtained. As a result, it can serve as an important basis for developing optimum controlling strategies of a DMFC [26]. The model can also predict the *remaining run-time* of a DMFC system under various operating conditions. Such information is also useful for practical situations.

2. Model description

The behavior of a fuel cell is closely related to its operating conditions, i.e. operating voltage (or current), operating temperature, fuel concentration, flow rates of fuel and air, and the pressure built in the anode and cathode chambers. In this paper, fuel concentration c, current density j, and operating temperature T are considered as the significant factors of the semi-empirical model for evaluating the DMFC efficiency ε_{dmfc} under steady-state conditions. In the following sections, preliminaries of the definitions and assumptions of ε_{dmfc} will be addressed first. Then a semi-empirical model of polarization behavior is proposed. By incorporating an algebraic semi-empirical model for fuel crossover evaluation, the

relationship between power density p_{dmfc} and efficiency ε_{dmfc} under various operating conditions is established.

2.1. Preliminaries

The ε_{dmfc} mainly consists of reversible thermodynamic efficiency ε_{thermo}, voltage efficiency of the fuel cell $\varepsilon_{voltage}$, and fuel utilization efficiency ε_{fuel} [3]. It can be written as:

$$\varepsilon_{dmfc} = \varepsilon_{thermo} \times \varepsilon_{voltage} \times \varepsilon_{fuel} \quad (1)$$

First, the reversible thermodynamic efficiency is defined as:

$$\varepsilon_{thermo} = \frac{\Delta g_{rxn}}{\Delta h_{rxn}} \quad (2)$$

where Δg_{rxn} and Δh_{rxn} are the changes of the Gibbs free energy and the enthalpy, respectively, of the reaction. When the assumption of an isobaric condition during the reaction is made, both the Gibbs free energy and the enthalpy of reaction are temperature dependent. Considering the oxidation reaction of a DMFC at anode:

$$CH_3OH + H_2O \rightarrow CO_2 + 6H^+ + 6e^- \quad (3)$$

and the reduction reaction at cathode:

$$\frac{3}{2}O_2 + 6H^+ + 6e^- \rightarrow 3H_2O \quad (4)$$

the ε_{thermo} of a DMFC is around 96.7–96.6% when T is within the range of 298 K to 340 K. For the reason of simplicity, we define ε_{thermo} = 96.7 % and neglect the temperature effect in the following illustration [3,27].

As for the voltage efficiency $\varepsilon_{voltage}$ of a fuel cell, it is defined as:

$$\varepsilon_{voltage} = \frac{V}{E_r} \quad (5)$$

where V and E_r denote the operating voltage and the thermodynamically reversible voltage, respectively, of a fuel cell. The effects of T and c on E_r can be evaluated using Nernst equation. It indicates that the E_r of a DMFC varies between about 1.20 V and 1.21 V at a standard pressure (1 atm) and a temperature between 298 K and 340 K, where the c is ranging from 0.75 M to 1.5 M. Both a higher c and a lower T will lead to a higher E_r. In this work, E_r = 1.21 V is employed under a feasible operating condition. One can modify E_r as a function of T and c by introducing Nernst equation [3]. Moreover, the operating voltage V will be interpreted as a function of T, c and j in Section 2.2.

Finally, the ε_{fuel} accounts the amounts of fuel that effectively generate electricity in the electrochemical reaction and the losses wasted due to fuel crossover. As a result, ε_{fuel} is expressed as:

$$\varepsilon_{fuel} = \frac{\dot{N}_{eff}}{\dot{N}_{eff} + \dot{N}_{mcr}} \quad (6)$$

where $\dot{N}_{eff}$ and $\dot{N}_{mcr}$ represent the molar fluxes of the effective fuel consumption and the fuel crossover losses, respectively. And $\dot{N}_{eff}$ can be addressed as a function of current density j.:

$$\dot{N}_{eff} = \frac{j}{zF} \quad (7)$$

where z = 6 for a DMFC, and F is the Faraday's constant. Moreover, the fuel crossover fluxes had been investigated in our previous work [25]. It will be briefly reviewed in Section 2.3.

2.2. Polarization model

Due to a variety of overpotentials, the actual operating voltage V of a fuel cell will always be lower than its E_r. There are various semi-empirical models in literature to depict the relationship between j and V of a fuel cell. The present work is based on the model proposed by Scott's group [18,19]:

$$V = E_r + b \log j_0 - b \log j - R_e j + C_1 \ln(1 - C_2 j) \quad (8)$$

where b, j_0 and R_e are the Tafel slope, the exchange current density and the area-specific resistance, in order. Meanwhile, C_1 and C_2 are empirically determined parameters regarding the mass transfer overpotential. The above model had been verified and was found to fit the behavior of PEMFCs and DMFCs very well. However, all the aforementioned parameters are T and c dependent [19]. The form of Eq. (8) itself cannot be used to predict the polarization behavior under various operating conditions, whereas it is essential for developing the controlling strategies of a fuel cell system. In this study, an additional term η_{cr} regarding the overpotential due to fuel crossover is added to Eq. (8). The relevant parameters logj_0, b, C_1, C_2 and η_{cr} are empirically approximated by cubic polynomials of T and c. Moreover, R_e is expressed as a temperature function. It is found that identifying R_e separately is helpful to enhance numerical stability and accuracy for the fitting procedures when various operating conditions are considered.

Since the V is generally measured by clamping the current collectors on both sides of the fuel cell stack (or single-cell module), the R_e can comprise the portions regarding ionic charge transport (mainly within the electrolyte membrane) and electronic charge transport (mainly induced between the interfaces of each components of the stack). Nonetheless, the ionic charge transport tends to be more difficult than electronic charge transport [3]. In our experiments where a single-cell DMFC module (35 mm × 35 mm MEA) is adopted, the electronic resistance (without MEA and gaskets in the testing module) was less than 7% of the resistance measured on a regular operating DMFC. The temperature range was between 303 K and 333 K. In addition, the tendency of the electronic resistance variation against the temperature is similar to that of the ionic resistance. Accordingly, the R_e in Eq. (8) is approximated by introducing the form of ionic conductivity σ of the electrolyte membrane and pursuing a *best fit* that can moderately incorporate the effect of electronic charge transport. The R_e can be expressed as:

$$R_e = \frac{\delta_m}{\sigma} \quad (9)$$

where δ_m is the thickness of the electrolyte membrane. The ionic specific conductivity of Nafion-type membrane (duPont de Nemours, Wilmington, DE) can be expressed as a function of T [28]:

$$\sigma(T) = (0.5139\lambda - 0.326) \exp\left[1268\left(\frac{1}{303} - \frac{1}{T}\right)\right] \quad (10)$$

where λ is the water content of a membrane. When the membrane is well-hydrated, the water content is constant and the ionic conductivity can be defined by the form of Eq. (10):

$$\sigma(T) = r_1 \exp\left(\frac{1268}{303} - \frac{r_2}{T}\right) \quad (11)$$

Because δ_m is known and R_e can be easily acquired while performing j–V measurements under various T r_1 and r_2 can then be determined using a nonlinear least-squares algorithm described in Appendix A. Consequently, $R_e(T)$ can be interpreted as:

$$R_e(T) = \frac{\delta_m}{r_1} \exp\left(\frac{r_2}{T} - \frac{1268}{303}\right) \quad (12)$$

The operating voltage of a DMFC can be influenced by the cathode mixed potential due to methanol crossover. It had been verified that the influence of methanol on the cathode mixed potential is independent of j [17]. Therefore, the η_{cr} as well as b, j_0, C_1 and C_2 are interpreted as functions of T and c Then Eq. (8) can be expressed

as:

$$V(T,c,j) = E_r + b(T,c)\cdot[a(T,c) - \log j] - R_e(T)\cdot j + C_1(T,c)\cdot\ln[1 - C_2(T,c)\cdot j] - \eta_{cr}(T,c) \quad (13)$$

where $a(T, c)$ is substituted for $\log[j_0(T, c)]$ to enhance numerical robustness of the fitting algorithm. The functions $a(T,c)$, $b(T,c)$, $C_1(T,c)$, $C_2(T,c)$ and $\eta_{cr}(T, c)$ are empirically approximated by cubic polynomials:

$$x_i(T,c) = \alpha_{1i} + \alpha_{2i}T + \alpha_{3i}c + \alpha_{4i}T^2 + \alpha_{5i}Tc + \alpha_{6i}c^2 + \alpha_{7i}T^3 + \alpha_{8i}T^2c + \alpha_{9i}Tc^2 + \alpha_{10i}c^3 \quad (14)$$

where x_i ($i = 1, 2, \ldots, 5$) can denote a, b, C_1, C_2 and η_{cr}. Each of the five functions consists of 10 parameters to be fitted. For a pre-assigned combination of (T_k, c_k), Eq. (13) can be expressed as:

$$V(T_k,c_k,j) = E_r + b_k\cdot[a_k - \log j] - R_e(T_k)\cdot j + C_{1,k}\cdot\ln\left[1 - C_{2,k}\cdot j\right] - \eta_{cr,k} \quad (15)$$

The j–V data corresponding to each (T_k, c_k) acquired experimentally was substituted into Eq. (15) to obtain parameters a_k, b_k, c_{1k}, c_{2k} and $\eta_{cr,k}$ using Levenberg–Marquardt algorithm, which was briefly illustrated in Appendix A. Based on a number of polarization measurements (for $k = 1, 2, \ldots, n$), the fitted results of Eq. (15) together with the corresponding (T_k, c_k) are then substituted into Eq. (14) to determine the unknown parameters a_{1i}, a_{2i}, …, a_{10i} using the ordinary least-squares method in Appendix B. Consequently, the operating voltage V can then be expressed by an explicit function of T, c and j, as was shown in Eqs. (12)–(14).

2.3. Methanol crossover model

Fuel crossover phenomenon is considered one of the most significant factors contributing to $\varepsilon_{\text{fuel}}$ of a DMFC. In our previous work [25], the methanol crossover flux was stated analytically in an algebraic function, which explicitly incorporated c, j and T of the fuel cell. The model took various physical parameters into account including the thicknesses of membrane, catalyst layer and gas diffusion layer (δ_m, δ_A, and δ_B), as well as electro-osmotic drag coefficient of methanol n_d and effective diffusivities (D_m, D_A and D_B) at the corresponding positions in a membrane electrode assembly (MEA). The transfer behavior of methanol was governed by diffusion and electro-osmosis. The aforementioned coefficients D_m, D_A, D_B and n_d were also expressed by functions of T and c. By adopting this methanol crossover model, the molar flux of the methanol crossover losses $\dot{N}_{\text{mcr}}$ in Eq. (6) can be expressed as:

$$\dot{N}_{\text{mcr}}(T,c,j) = -j\cdot c_{2,m}(c,j,T)\cdot D_m(T)\cdot\kappa(T)\frac{\exp\left[j\delta_m\kappa(T)\right]}{1 - \exp\left[j\delta_m\kappa(T)\right]} \quad (16)$$

where

$$c_{2,m}(T,c,j) = \frac{K_2\left\{-1 + \exp\left[j\delta_m\kappa(T)\right]\right\}\left\{D_B(T)\left[12FcK_1D_A(T) - j\delta_A\right] - 2jK_1\delta_BD_A(T)\right\}}{12F\left\{-D_A(T)D_B(T) + \exp\left[j\delta_m\kappa(T)\right]\left\{D_A(T)D_B(T) + jK_2D_m(T)\kappa(T)\left[\delta_AD_B(T) + K_1\delta_BD_A(T)\right]\right\}\right\}} \quad (17)$$

is the methanol concentration at the interface between the anode catalyst layer and the membrane, K_1 and K_2 are partition coefficients, while effective diffusivities D_A, D_B and D_m are all functions of temperature T. Moreover

$$\kappa = \frac{n_d(T)\cdot s}{D_m(T)\cdot F} \quad (18)$$

is defined for the simplicity of the equation expression, where the concentration translation factor $s = 18.4$ is employed for diluted methanol aqueous solution.

According to the model, the functions $D_A(T)$, $D_B(T)$, $D_m(T)$ and $n_d(T)$ are defined as:

$$D_A(T) = \beta_1\ \exp\left[\beta_2\left(\frac{1}{353} - \frac{1}{T}\right)\right] \quad (19)$$

$$D_B(T) = \beta_3\times 10^{-1.4163-\beta_4/T} \quad (20)$$

$$D_m(T) = \beta_5\ \exp\left[\beta_6\left(\frac{1}{333} - \frac{1}{T}\right)\right] \quad (21)$$

and

$$n_d(T) = 2.9\ \exp\left[\beta_7\left(\frac{1}{\beta_8} - \frac{1}{T}\right)\right] \quad (22)$$

In Eqs. (19)–(22), there are eight unknown parameters β_i ($i = 1, 2, \ldots, 8$) to be fitted by adopting the Levenberg–Marquardt algorithm described in Appendix A. Once the eight fitted parameters are determined, the quantitative prediction of the $\dot{N}_{\text{mcr}}(T, c, j)$ will be straightforward with no need of any numerical strategy.

2.4. Power–efficiency relationship

Based on the aforementioned illustration, the $\varepsilon_{\text{dmfc}}$ can then be expressed by an explicit function of operating variables T, c and j:

$$\varepsilon_{\text{dmfc}}(T,c,j) = 96.7\%\times\frac{V(T,c,j)}{1.21}\times\frac{j/6F}{(j/6F)\cdot\dot{N}_{mcr}(T,c,j)} \quad (23)$$

In addition, the power density of a DMFC can be expressed as:

$$p_{\text{dmfc}}(T,c,j) = j\cdot V(T,c,j) \quad (24)$$

By incorporating Eqs. (23) and (24), a clear picture that simultaneously depicts the relationships between the performance indices ($\varepsilon_{\text{dmfc}}$ and p_{dmfc}) and the operating variables (T, c and j) is revealed.

Furthermore, the remaining run-time of a DMFC can be predicted from $\varepsilon_{\text{dmfc}}$ and p_{dmfc} by:

$$t_r(T,c,j) = \frac{n_f\cdot\Delta h_{\text{rxn}}\cdot\varepsilon_{\text{dmfc}}(T,c,j)}{p_{\text{dmfc}}(T,c,j)\cdot A\cdot 3600} \quad (25)$$

where n_f and A are the remaining amount of fuel in the fuel tank and the effective area of the MEA, respectively. It can be alternatively defined based on unit mole of the fuel and the specific area of the MEA as:

$$\tilde{t}_r(T,c,j) = \frac{\Delta h_{\text{rxn}}\cdot\varepsilon_{\text{dmfc}}(T,c,j)}{p_{\text{dmfc}}(T,c,j)\cdot 3600} \quad (26)$$

Such information varies with operating conditions and is generally useful for practical situations.

3. Experimental

The experiment of the present work consists of two parts. One is the j–V measurements for fitting and validation of the proposed polarization model. The other is the methanol crossover measurements for establishing the semi-empirical methanol crossover model and thereby the relationship between $\varepsilon_{\text{dmfc}}$ and p_{dmfc} defined by Eqs. (23) and (24).

3.1. Experimental facilities

The experimental facilities employed in this study were the same as those described in [25]. A standard testing module of a unit commercial MEA (35 mm × 35 mm, duPont de Nemours,

Table 1
A brief list of the experimental conditions for the fitting and the validation of the proposed polarization model.

Items	Descriptions
1. MEA	35 mm × 35 mm (DuPont Nation® 117)
2. Graphite channel type	Single serpentine, 1 mm in width and depth
3. Operating temperature for model fitting	303 K, 313 K, 323 K, 333 K
4. Fuel concentration for model fitting	0.75 M, 1.0 M, 1.25 M, 1.5 M
5. Conditions for model validation	(a) 313 K: 0.875 M, 1.125 M, 1.375 M (b) 1.0 M: 308 K, 318 K, 328 K
6. Electric load	Potentiostatic mode from 0.6 V to 0.15 V with an increment of −0.05 V and the duration of 5 min for each measurement
7. Fixed gas flow rate on the cathode side	Feeding air with 150 mL min^{-1}
8. Fixed fuel flow rate on the anode side	5 mL min^{-1}
9. Fuel delivery type	Single pass

Wilmington, DE) was adopted for the experiments. The MEA was Nafion-117 based. The anode catalyst was Pt–Ru/C (Pt–Ru content 40 wt%, Pt/Ru wt ratio was 1/1) and the cathode catalyst was Pt/C (Pt content 40 wt%). The Pt loadings at anode and cathode of the MEA were both 2 mg cm^{-2}. The flow channel was single serpentine and 1 mm in width and depth. A temperature control unit was applied to provide appropriate temperature conditions. The fuel delivery was driven by a precision liquid pump (Eyela MP-1000, Tokyo, Japan). In order to keep a constant fuel concentration, the fuel delivery was single pass without circulating back to the fuel tank. To avoid the influence of uncertainties and variation of CO_2 concentration in the atmosphere, the air fed into cathode was provided by a gas cylinder. The exhausted stream at the cathode outlet was guided into a gas chromatography (China Chromatography GC3000, Taipei, Taiwan) with a thermal conductivity detector (TCD) for CO_2 measurement. A source meter (Keithley 2440, Cleveland, OH) was introduced to provide designate electric loads. In addition, a precision internal resistance meter (Hioki 3561, Nagano, Japan) was adopted to measure the area-specific resistance of the fuel cell by clamping the current collectors on both sides of the single-cell module.

3.2. *j–V* data acquisition for the polarization model

Four levels of T and c were assigned for j–V measurements as shown in Table 1. There were 16 combinations of (T_k, c_k) with $k = 1, 2, \ldots, 16$. The j–V measurements were carried out by the potentiostatic technique with voltages ranged from 0.6 V to 0.15 V and a decrement of 0.05 V. The duration of each measurement was 5 min. Thus, 10 data points for each j–V measurement were obtained. The flow rates of air and fuel were 150 mL min^{-1} and 5 mL min^{-1}, respectively. The internal resistance corresponding to each (T_k, c_k) was also acquired for the fitting of the polarization curve. The resulting data were then introduced to establish the polarization model following the procedure described in Section 2.2.

To validate the resulting polarization model, additional six j–V measurements were carried out at a constant $T = 313$ K with $c = 0.875$ M, 1.125 M and 1.375 M, and at a constant $c = 1.0$ M with $T = 308$ K, 318 K and 328 K. These measured data were compared with the estimated results using the resulting polarization model to verify its feasibility.

3.3. CO_2 measurements for the methanol crossover model

Methanol crossover measurements were carried out using the same procedures as those described in [25]. Although most of the methanol that transmits to cathode can be oxidized to CO_2, there are possibilities that some methanol may remain unreacted and induce certain intermediates. Many researchers assumed that the amount of the unreacted methanol was negligible when comparing with the overall crossover methanol [24,29], whereas Eccarius et al. suggested the residual methanol cannot be omitted in some cases [22]. Therefore, the effect of the residual methanol on the crossover evaluation is still an open issue. Moreover, the induced intermediates are generally neglected, since the amounts are very small and the reaction rates are fast [30]. In our previous work [25], the influence of CO on the methanol crossover measurement was verified to be less than 1%. Accordingly, it is assumed in this paper that all the methanol that transmits to cathode is instantaneously oxidized to CO_2 and HO_2, and the intermediates such as CO, CH_2OH and CHOH are neglected. The methanol crossover fluxes can be quantitatively identified by measuring the CO_2 concentration of the cathode outlet exhausted stream. A brief list of the experimental conditions for establishing the methanol crossover model was shown in Table 2. Two levels of T and c were assigned, thus obtaining four sets of T and c combinations. For each set of T and c, 7 levels of j equally distributed within the feasible region were assigned. The electric load was applied by the galvanostatic mode. Accordingly, there were 28 sets of CO_2 molar fluxes to be acquired for an operating DMFC.

Nonetheless, not only the methanol but also the CO_2 produced at the anode can permeate across the membrane to cathode. Such amount of CO_2 should be subtracted from the CO_2 measurement results in an operating DMFC to identify the methanol crossover fluxes more accurately. The half-cell measurement scheme was then introduced to measure the CO_2 crossover fluxes [22,25,31], where the air flow on the cathode side was alternatively replaced by an inert gas such as nitrogen, and the specified currents were drawn by a source meter. In such situations, even some methanol

Table 2
A brief list of the experimental conditions for the fitting and the validation of the crossover model.

Items	Descriptions
1. Operating temperature for model fitting	303 K, 333 K
2. Fuel concentration for model fitting	1.0 M, 2.0 M
3. Conditions for model validation	1.5 M: 303 K, 313 K, 323 K, 333 K
4. Electric load	Assigning 7 levels of current density equally distributed within the feasible region corresponding to each combination of temperature and concentration
5. Fixed gas flow rate on the cathode side	150 mL min^{-1} (feeding N_2 for half-cell measurement, air for ordinary DMFC measurement)
6. Fixed fuel flow rate on the anode side	5 mL min^{-1}
7. Fuel delivery type	Single pass

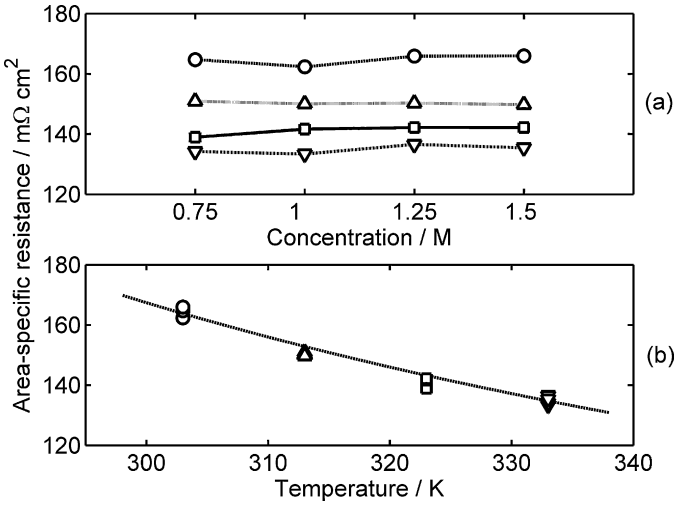

Fig. 1. The area-specific resistances: (a) the measured values under various levels of fuel concentration and operating temperature: (○) 303 K, (△) 313 K, (□) 323 K and (▽) 333 K; (b) the measured values (symbols) and the fitted results (curve).

transmitted through the membrane from anode to cathode, it did not perform any reaction due to the lack of oxygen. Therefore, no any additional CO_2 was produced at cathode. If any CO_2 was detected at the cathode outlet under such operating modes, it was recognized as that transmitted from anode, thereby verifying the CO_2 crossover fluxes. The CO_2 crossover fluxes in the half-cell mode were also measured according to the same conditions listed in Table 2. Accordingly, the methanol crossover fluxes could be obtained for fitting the eight unknown parameters β_i (i = 1, 2, . . ., 8).

It is noted that the CO_2 crossover fluxes in half-cell measurements may not be identical to that in an ordinary operating DMFC, thus influencing the compensation of the methanol crossover measurement. The CO_2 concentrations at the anodes of both cases are the same, whereas the CO_2 concentration at the cathode under the half-cell condition may be lower than that under the ordinary operating condition. It is because CO_2 can be generated at the cathode under the ordinary operating condition only. Fortunately, such a deviation between the cathode CO_2 concentrations of both cases is negligible when the methanol crossover is slight. When the methanol crossover is severer, our previous work has verified that the CO_2 crossover becomes less significant when comparing with the methanol crossover [25]. Accordingly, the difference of CO_2 crossover between half-cell and ordinary operating conditions is neglected in this work, as was assumed in the literatures [22,31].

Finally, to validate the proposed efficiency model, four sets of additional methanol crossover measurements were carried out at a constant c = 1.5 M with T = 303 K, 313 K, 323 K and 333 K. For each measurement condition, the corresponding j–V measurements were also performed to determine ε_{dmfc} and p_{dmfc} for the comparison with the estimated results using the achieved efficiency model.

4. Results and discussions

4.1. Polarization model

By following the procedure described in Section 3.2, a total of 160 j–V data were acquired. For each combination of (T_k, c_k), the internal resistance was also obtained and shown in Fig. 1(a). It revealed that the internal resistance of an operating DMFC was independent of c, whereas higher T led to lower internal resistances. The results shown in Fig. 1(a) were inserted into Eq. (12)

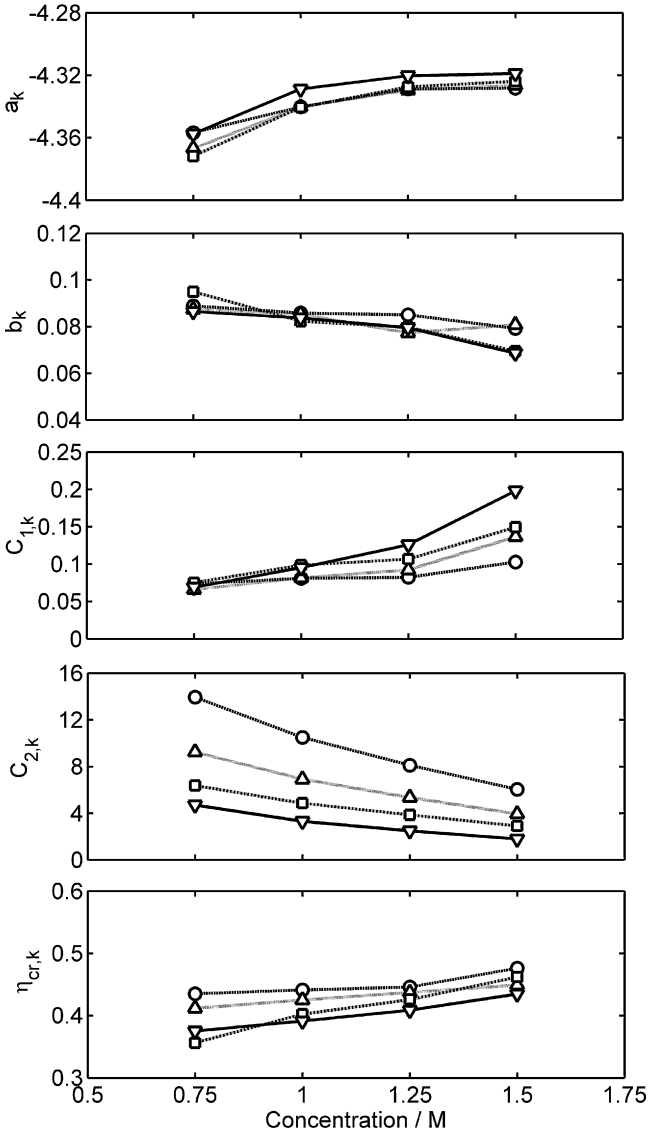

Fig. 2. The fitted values of the parameters in Eq. (15) corresponding to various levels of methanol concentration c and operating temperature: (○) 303 K, (△) 313 K, (□) 323 K and (▽) 333 K.

to obtain the parameters $r_1 = 1.46 \times 10^{-2}\ \Omega^{-1}\ cm^{-1}$ and r_2 = 656.41 K as δ_m = 0.018 cm. The experimental data and the fitting results of Eq. (12) are shown in Fig. 1(b). The relative error between the experimental data and the estimated values was around 1.3%. Such a temperature dependent function $R_e(T)$ was then employed in Eqs. (13) and (15).

For each combination of (T_k, c_k), the corresponding 10 j–V data were inserted into Eq. (15) to obtain the parameters a_k, b_k, C_{1k}, C_{2k} and $\eta_{cr,k}$ for k = 1, 2, . . ., 16. The fitting results of these parameters are illustrated in Fig. 2. All these values together with each individual combination of (T_k, c_k) were introduced to Eq. (14) to obtain the parameters $a_{1i}, a_{2i}, \ldots, a_{10i}$ (i = 1, 2 , . . ., 5) by means of linear least squares method described in Appendix B. The form of these functions and the values of the fitted parameters are summarized in Table B.1. Accordingly, the semi-empirical polarization model of a DMFC under various operating conditions was then accomplished.

The resulting model was validated using additional six sets of j–V measurements obtained according to the T and c listed in Table 1. Fig. 3 shows the polarization curves calculated using Eq. (13) under various operating temperatures with a fuel concentration of 1.0 M.

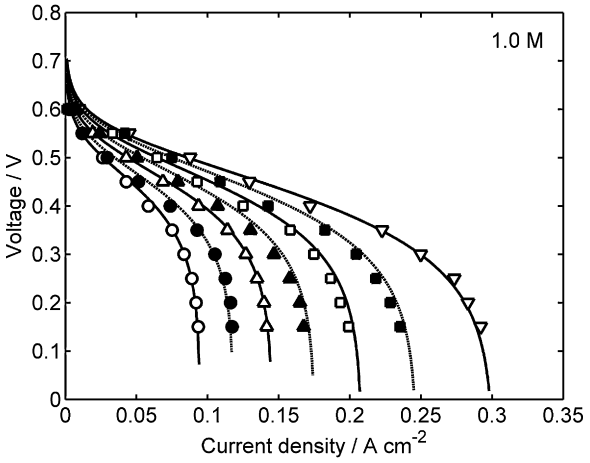

Fig. 3. Polarization curves based on experimental results (symbols) and the proposed model (curves). The fuel concentration is 1.0 M. The operating temperatures are: (○) 303 K, (●) 308 K, (△) 313 K, (▲) 318 K, (□) 323 K, (■) 328 K and (▽) 333 K.

The empty symbols represent the experimental data that were employed for fitting the unknown parameters, while the filled symbols are the additional data for model validation. It can be observed that the prediction of the proposed model meets the experimental data quite well. The relative deviation between the predicted and the measured voltages was around 3.3%. Similarly, the proposed model was also validated under various concentration levels. Fig. 4 shows the polarization curves with the fuel concentration ranging from 0.75 M to 1.5 M, whereas the operating temperature was kept at 313 K. It reveals a good coincidence between the predicted and the measured results. The relative deviation between the predictive and measured data was around 2.1%. Consequently, the feasibility of the proposed polarization model can be verified.

4.2. Power–efficiency relationship

Using the semi-empirical methanol crossover model described in Section 2.3 and the procedures mentioned in Section 3.3, an illustration of $\dot{N}_{mcr}(T, c, j)$ in the space of multi-operating variables was obtained and shown in Fig. 5. The $V(T, c, j)$ obtained in Section 4.1 and $\dot{N}_{mcr}(T, c, j)$ obtained in this section were then introduced to

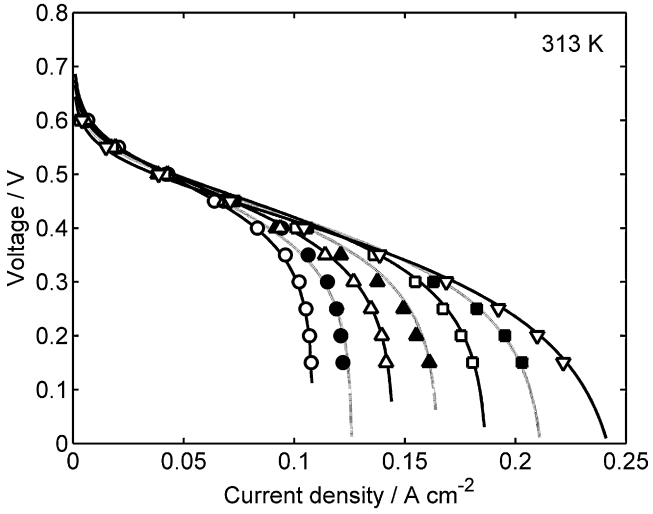

Fig. 4. Polarization curves based on experimental results (symbols) and the proposed model (curves). The operating temperature is 313 K. The fuel concentrations are: (○) 0.75 M, (●) 0.875 M, (△) 1.0 M, (▲) 1.125 M, (□) 1.25 M, (■) 1.375 M, and (▽) 1.5 M.

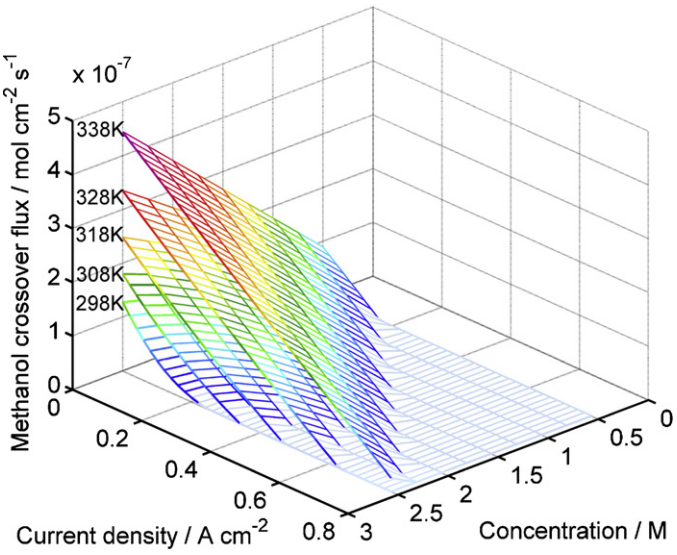

Fig. 5. An illustration of methanol crossover fluxes in the (T, c, j) space.

Eq. (23) to calculate ε_{dmfc}. An illustration of the $\varepsilon_{dmfc}(T, c, j)$ in the space of multi-operating variables is depicted in Fig. 6. A complex and highly nonlinear behavior coupled with multi-variables is observed. It therefore reveals the essentiality of the proposed model that provides a clear picture of ε_{dmfc} influenced by various operating variables. A special situation at 333 K is extracted from Fig. 6 to illustrate the influence of c on ε_{dmfc} and is shown in Fig. 7. An increasing ε_{dmfc} with j is observed in the lower j region. It is because the methanol crossover fluxes are attenuated by an increase in current density, thus enhancing the fuel utilization efficiency. On the other hand, a decrease of ε_{dmfc} with j is observed in the higher J region. It is because the operating voltage is lowered when approaching the limiting current density, which leads to a decrease in voltage efficiency. Fig. 7 also indicates that a higher methanol concentration may lead to a larger current density. However, the maximum ε_{dmfc} is suppressed.

By introducing the $V(T, c, j)$ function obtained in Section 4.1 into Eq. (24), the $p_{dmfc}(T, c, j)$ in the multi-dimensional variable space was obtained and shown in Fig. 8. With the operating temperature

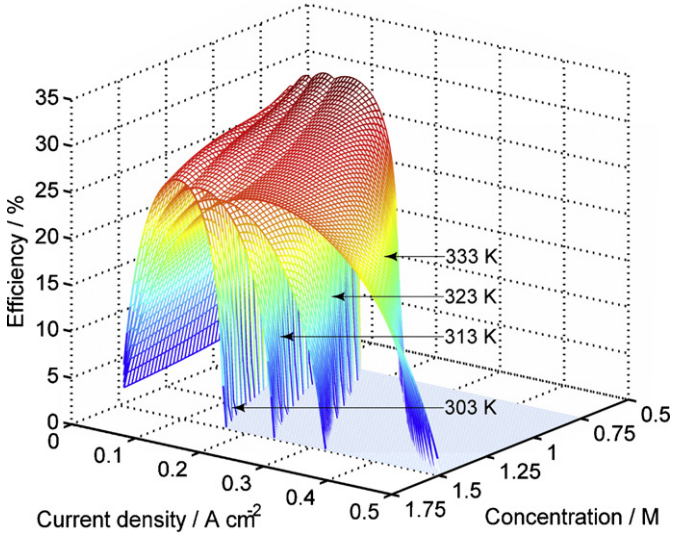

Fig. 6. An illustration of the efficiency of a DMFC in the (T, c, j) space.

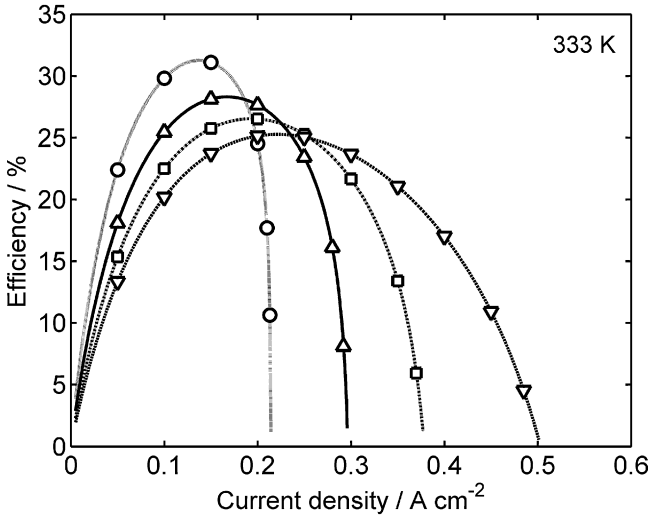

Fig. 7. The j–ε_{dmfc} curves with various fuel concentrations. The operating temperature is 333 K, while the fuel concentrations are: (○) 0.75 M, (△) 1.0 M, (□) 1.25 M, and (▽) 1.5 M.

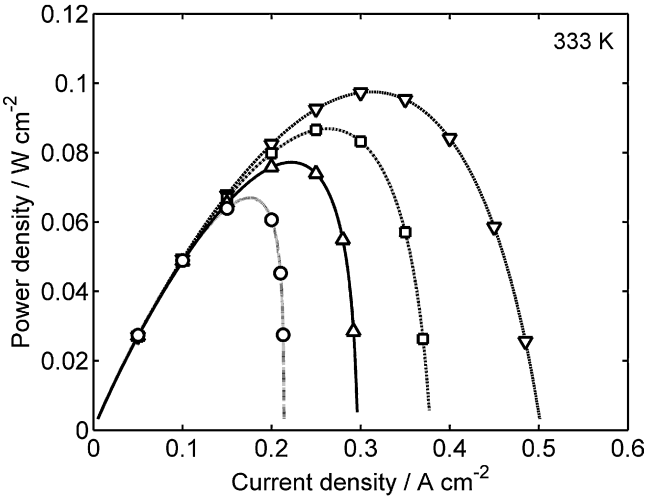

Fig. 9. The j–p_{dmfc} curves with various fuel concentrations. The operating temperature is 333 K, while the fuel concentrations are: (○) 0.75 M, (△) 1.0 M, (□) 1.25 M, and (▽) 1.5 M.

being 333 K, the j–p_{dmfc} curves are depicted in Fig. 9 to illustrate the influence of fuel concentration on p_{dmfc}. It is observed that in the region of c = 0.75–1.5 M, a higher fuel concentration leads to increases both in highest j and maximum p_{dmfc}.

Finally, the $\varepsilon_{dmfc}(T, c, j)$ and the $p_{dmfc}(T, c, j)$ defined in Eqs. (23) and (24), respectively, are illustrated simultaneously. Additional four sets of j–V and methanol crossover measurement data were introduced to validate the p_{dmfc}–ε_{dmfc} relationship depicted by the semi-empirical model. The results are shown in Fig. 10 and the *leaf-shaped* curves are observed. The symbols in Fig. 10 represent the experimental data, while the curves are calculated using the semi-empirical model of Eqs. (23) and (24). A total of 28 points were evaluated that shows a good coincidence between the predicted results and the experimental data. The relative error regarding the p_{dmfc} data was within 2.2% and that regarding the ε_{dmfc} data was within 0.8%. Accordingly, the proposed models are verified to be capable of describing the relationship between p_{dmfc} and ε_{dmfc} of a DMFC under various operating conditions.

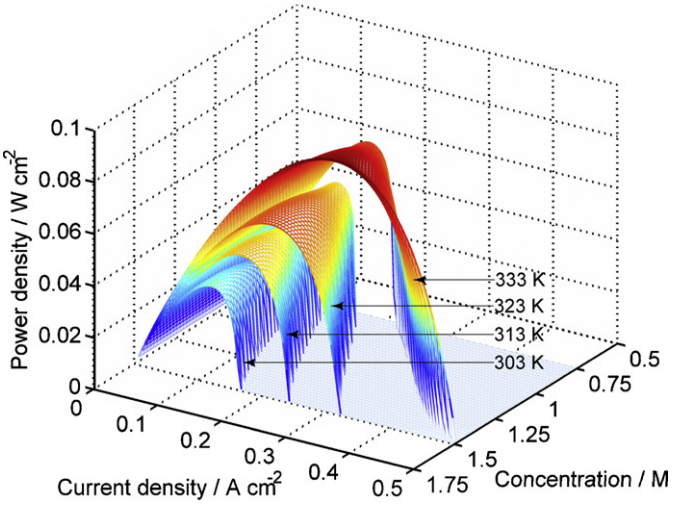

Fig. 8. An illustration of the power density of a DMFC in the (T, c, j) space.

4.3. Further discussions

One of the major objectives of this paper is to depict the performance indices (p_{dmfc} and ε_{dmfc}) and the operating variables (T, c, and j), sin one diagram. The p_{dmfc} and the ε_{dmfc} are expressed by explicit functions of (T, c, and j) It is evident that the operating range of current density varies with temperature and fuel concentration. On the other hand, the operating voltages always range between zero and the thermodynamically reversible voltage. It is more intuitive to estimate the voltage efficiency using operating voltage rather than current density. Therefore, the operating voltages instead of current densities are designated on the p_{dmfc}–ε_{dmfc} curves to indicate the influence of the electric load on these two performance indices. Whenever a specific voltage is assigned, the current density can be estimated from Eq. (13) by adopting the Newton–Raphson algorithm and then substituted into Eqs. (23) and (24) to obtain p_{dmfc} and ε_{dmfc} for power density and efficiency evaluation.

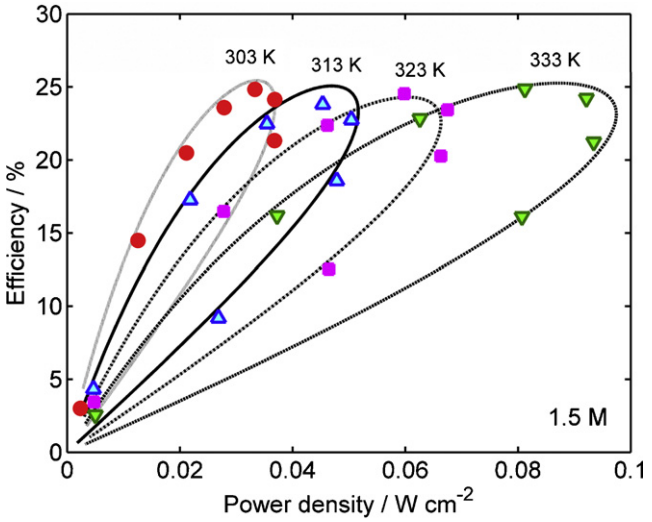

Fig. 10. The p_{dmfc}–ε_{dmfc} relationship calculated from semi-empirical model (curves) and the experimental data (symbols) for model validation. The fuel concentration is 1.5 M. The operating temperatures are: (●) 303 K, (▲) 313 K, (■) 323 K, and (▼) 333 K.

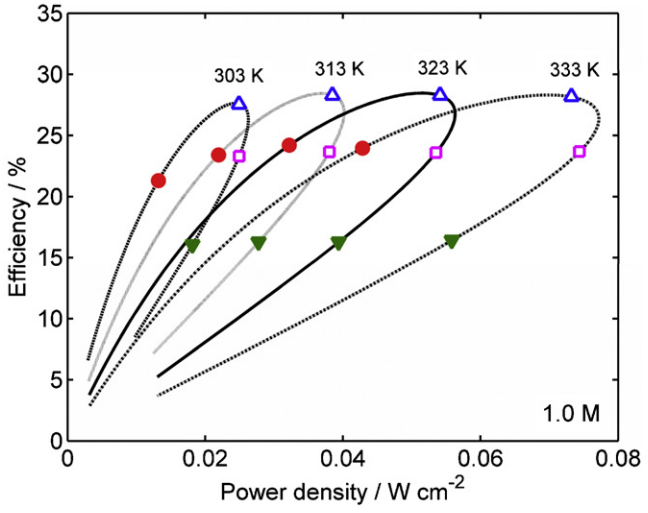

Fig. 11. The p_{dmfc}–ε_{dmfc} curves under various operating temperatures. The fuel concentration is 1.0 M. The symbols indicate the corresponding operating voltages: (●) 0.5 V, (△) 0.4 V, (□) 0.3 V, and (▼) 0.2 V.

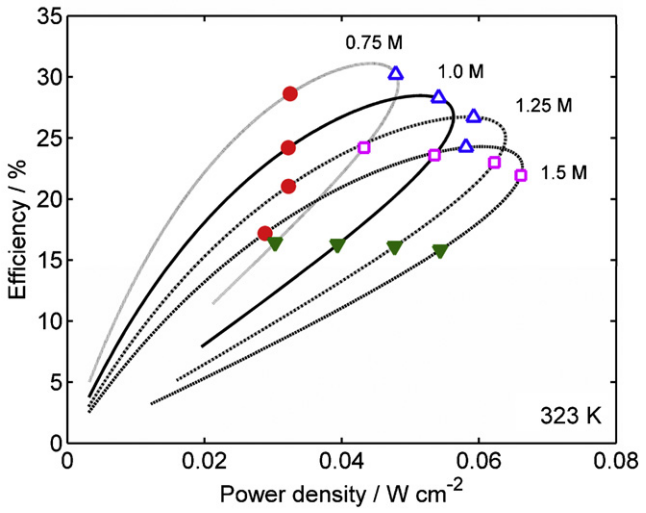

Fig. 12. The p_{dmfc}–ε_{dmfc} curves with various fuel concentrations. The operating temperature is 323 K. The symbols indicate the corresponding operating voltages: (●) 0.5 V, (△) 0.4 V, (□) 0.3 V, and (▼) 0.2 V.

Fig. 11 shows p_{dmfc}–ε_{dmfc} curves at various operating temperatures and a fuel concentration of 1.0 M. The (p_{dmfc}–ε_{dmfc}) data points corresponding to four levels of operating voltages are also designated on the curves. Each curve intersects at the origin of p_{dmfc}–ε_{dmfc} diagram. Although the origin corresponds to the open-circuit voltage and a maximum value of voltage efficiency, it also indicates the current density is zero; hence both p_{dmfc} and ε_{dmfc} are zero. The decrease of an operating voltage from open-circuit voltage to a lower voltage results in a decrease in voltage efficiency, whereas the current density is increased which leads to an increase in the fuel utilization efficiency. Therefore, the p_{dmfc}–ε_{dmfc} diagram shows a positive tendency. Along a leaf-shaped curve in the clockwise direction, an ultimate ε_{dmfc} is achieved and followed by a decrease in ε_{dmfc} because the decreasing voltage significantly lowers the resulted values of ε_{dmfc} and p_{dmfc}. Eventually, the p_{dmfc}–ε_{dmfc} relationship is back to the origin of the diagram when operating voltage approaches zero. In practice, only the operating conditions regarding the *upper-left* portion of the curve are considered since they always achieve a higher efficiency within a feasible power domain.

In Fig. 11, the preferable value of the operating voltage is around 0.4 V since both p_{dmfc} and ε_{dmfc} approach ultimate values. It is also observed that increasing the operating temperature is beneficial to enhance the power density of a DMFC without reducing its maximum ε_{dmfc}. However, under a constant p_{dmfc}, increasing operating temperature could reduce ε_{dmfc} due to the decrease in fuel utilization efficiency. Another example regarding the effect of fuel concentration on the p_{dmfc}–ε_{dmfc} relationship is shown in Fig. 12, in which the operating temperature is kept at 323 K. It indicates the maximum ε_{dmfc} occurs at about 0.4 V, whereas the maximum p_{dmfc} is within a range of 0.3–0.4 V. A higher level of fuel concentration causes an increase in p_{dmfc}. Nonetheless, higher fuel concentration also leads to severer fuel crossover, thus significantly suppressing ε_{dmfc}.

The remaining run-time $t_r(T, c, j)$ is another index of interest for a fuel cell system. Fig. 13 shows the plots of specific remaining run-time $\tilde{t}_r(T, c, j)$ against p_{dmfc} as defined in Eq. (26). The operating conditions were the same as those shown in Fig. 11. Followed by a decrease in the operating voltage, the $\tilde{t}_r$ shows a dramatic drop to a level corresponding to the maximum p_{dmfc}. Then it tends to approach a stabilized value that corresponds to the situation where the limiting current density occurs. It is noted that both the p_{dmfc}–ε_{dmfc} relationship and the remaining run-time are coupled

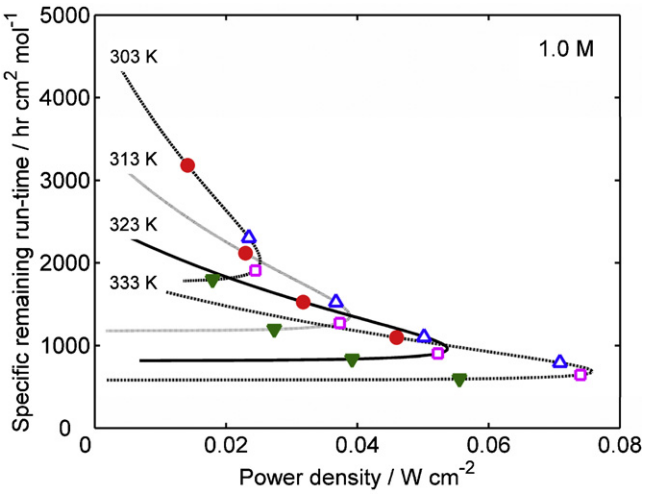

Fig. 13. The specific remaining run-time under various operating temperatures and a fuel concentration of 1.0 M. The corresponding operating voltages are: (●) 0.5 V, (△) 0.4 V, (□) 0.3 V, and (▼) 0.2 V.

with operating T, c and j (or V) simultaneously. When considering ε_{dmfc} and $\tilde{t}_r$, a fuel cell does not always operate at the condition that a maximum power is delivered. In a more realistic situation, a feasible power demand is given for a controlling strategy to pursue its optimum value of efficiency. Therefore, how to determine the combination of operating (T, c, and j) (or V) is crucial to a DMFC system. The model described in Eqs. (23) and (24) will serve as an important basis for this purpose [26].

5. Conclusions

A semi-empirical model for efficiency evaluation of a DMFC has been proposed. The power density and the efficiency of a DMFC have been represented by explicit functions of operating temperature, fuel concentration, and current density. It is illustrated to be capable of depicting performance indices and operating variables in a diagram. It provides a good prediction and a clear insight into these relationships. The experimental validation of the proposed model is also verified. Moreover, the remaining run-time of the system under various operating conditions can be estimated

Table A.1
The corresponding parameters and functions concerning Levenberg–Marquardt algorithm.

Unknown parameters	q	Estimated functions	Corresponding equations	Measured data	p
$\boldsymbol{\Theta} = [\ r_1 \quad r_2\ ]^T$	2	$f = R_e$	Eq. (12)	Area-specific resistance	16
$\boldsymbol{\Theta} = [\ a_k \quad b_k \quad C_{1,k} \quad C_{2,k} \quad \eta_{cr,k}\ ]^T$	5	$f = V$	Eq. (15)	Operating voltage	10
$\boldsymbol{\Theta} = [\ \beta_1 \quad \beta_2 \quad \cdots \quad \beta_8\ ]^T$	8	$f = \dot{N}_{mcr}$	Eqs. (16)–(22)	Methanol crossover flux	28

Table B.1
A brief summary of the fitting parameters defined in Eq. (14).

Parameters	Fitting results									
$x_i(T,c)$[a]	α_{1i}	α_{2i}	α_{3i}	α_{4i}	α_{5i}	α_{6i}	α_{7i}	α_{8i}	α_{9i}	α_{10i}
$a(T, c)$	−4.40	−0.25	0.38	−0.23	1.19	−0.94	0.27	−0.48	−0.36	0.49
$b(T, c)$	0.15	−0.02	−0.31	0.07	−0.06	0.59	−0.07	0.14	−0.19	−0.27
$C_1(T, c)$	−0.48	0.12	3.21	0.09	−1.06	−5.61	−0.12	0.39	0.85	3.20
$C_2(T, c)$	88.07	−159.70	−137.99	125.11	125.60	112.44	−35.96	−48.79	−22.83	−48.10
$\eta_{cr}(T, c)$	0.59	−0.72	0.35	−0.20	2.27	−2.10	0.38	−1.01	−0.49	1.52

[a] $x_i(T, c) = \alpha_{1i} + \alpha_{2i}T + \alpha_{3i}c + \alpha_{4i}T^2 + \alpha_{5i}Tc + \alpha_{6i}c^2 + \alpha_{7i}T^3 + \alpha_{8i}T^2c + \alpha_{9i}Tc^2 + \alpha_{10i}c^3$.

by introducing the proposed model. It is generally essential to practical situations. Since the model is stated in the form of an analytical function, the quantitative prediction of power density and efficiency is straightforward whenever the relevant parameters in the model are pre-determined. Consequently, it can serve as an important basis for developing controlling strategies of a DMFC system.

Acknowledgements

This research project was financially supported by the National Science Council, Taiwan, R.O.C. (NSC 98-2221-E-149-009). The authors are grateful to the reviewers for valuable comments. The assistance in experiments by Mr. Tsung-Han Li and Mr. Jin-Wei Yang is also appreciated.

Appendix A. The nonlinear least-squares algorithm

The well-known Levenberg–Marquardt algorithm is adopted for the fitting of the unknown parameters in this paper. Let $\Theta = [\ \theta_1 \quad \theta_2 \quad \cdots \quad \theta_q\ ]^T$, $\mathbf{y} = [\ y_1 \quad y_2 \quad \cdots \quad y_p\ ]^T$, and $\mathbf{f} = [\ f_1 \quad f_2 \quad \cdots \quad f_p\ ]^T$ denote the unknowns to be fitted, the measured data, and the estimated results by the model, in order. Based on an initial guess of $\Theta^{(0)}$ and p sets of measurements, the key of the algorithm is to determine the next search of the unknowns as the followings:

$$\Theta^{(l)} = \Theta^{(l-1)} + [\mathbf{J}^{(l-1)^T}\mathbf{J}^{(l-1)} + \alpha^{(l-1)}\mathbf{I}_q]^{-1}\mathbf{J}^{(l-1)^T}(\mathbf{y} - \mathbf{f}^{(l-1)}) \tag{A.1}$$

where $\alpha^{(l-1)}$, $\mathbf{I}_q$ and l are relaxation factor, identity matrix and iteration index, in order. Furthermore, the Jacobian matrix $\mathbf{J}$ is defined as:

$$\boldsymbol{J} = \begin{bmatrix} \frac{\partial f_1}{\partial \theta_1} & \frac{\partial f_1}{\partial \theta_2} & \cdots & \frac{\partial f_1}{\partial \theta_q} \\ \frac{\partial f_2}{\partial \theta_1} & \frac{\partial f_2}{\partial \theta_2} & \cdots & \frac{\partial f_2}{\partial \theta_q} \\ \vdots & \vdots & \ddots & \vdots \\ \frac{\partial f_p}{\partial \theta_1} & \frac{\partial f_p}{\partial \theta_2} & \cdots & \frac{\partial f_p}{\partial \theta_q} \end{bmatrix} \tag{A.2}$$

It is noted that the finite difference approximation is introduced for Eq. (A.2) when the analytical form of $\mathbf{J}$ cannot be obtained. By Eq. (A.1), the unknowns are updated in each iteration of the algorithm until $\Theta^{(l)}$ approaches $\Theta^{(l-1)}$ adequately. One can refer to [32] for more details of the algorithm. The proposed parameters and functions concerning Levenberg–Marquardt algorithm are summarized in Table A.1.

Appendix B. The ordinary least-squares estimate

The unknown parameters $\alpha_{1i}, \alpha_{2i}, \ldots, \alpha_{10i}$ defined in Eq. (14) can be estimated by ordinary least-squares method. When a number of (T_k, c_k) are assigned and the corresponding parameters $x_{i,k}$ (*i.e.* a_k, b_k, c_{1k}, c_{2k}, and $\eta_{cr,k}$) are determined by Levenberg–Marquardt algorithm, Eq. (14) can be expressed by a matrix form:

$$\mathbf{X}_i = \mathbf{M} \cdot \mathbf{A}_i \tag{B.1}$$

where $\mathbf{X}_i = [\ x_{i,1} \quad x_{i,2} \quad \cdots \quad x_{i,n}\ ]^T$, $\mathbf{A}_i = [\ \alpha_{1i} \quad \alpha_{2i} \quad \cdots \quad \alpha_{10i}\ ]^T$, and

$$\mathbf{M} = \begin{bmatrix} 1 & T_1 & c_1 & T_1^2 & T_1c_1 & c_1^2 & T_1^3 & T_1^2c_1 & T_1c_1^2 & c_1^3 \\ 1 & T_2 & c_2 & T_2^2 & T_2c_2 & c_2^2 & T_2^3 & T_2^2c_2 & T_2c_2^2 & c_2^3 \\ \vdots & \vdots & \vdots & \vdots & \vdots & \vdots & \vdots & \vdots & \vdots & \vdots \\ 1 & T_n & c_n & T_n^2 & T_nc_n & c_n^2 & T_n^3 & T_n^2c_n & T_nc_n^2 & c_n^3 \end{bmatrix} \tag{B.2}$$

It is noted that $n = 16$ in the illustrated examples of this article. Then the ordinary least-squares estimate of $\mathbf{A}_i$ can be expressed as [32]:

$$\mathbf{A}_i = (\mathbf{M}^T\mathbf{M})^{-1}\mathbf{M}^T \cdot \mathbf{X}_i \tag{B.3}$$

The fitting results of Eq. (14) are summarized in Table B.1.

References

[1] F. Barbir, T. Gómez, International Journal of Hydrogen Energy 21 (1996) 891–901.
[2] R.S. Gemmen, C.D. Johnson, Journal of Power Sources 159 (2006) 646–655.
[3] R. O'Hayre, S.W. Cha, W. Colella, F.B. Prinz, Fuel Cell Fundamentals, John Wiley & Sons, New Jersey, 2006.
[4] J. Cruickshank, K. Scott, Journal of Power Sources 70 (1998) 40–47.
[5] R. Jiang, D. Chu, Journal of the Electrochemical Society 151 (2004) A69–76.
[6] R. Jiang, C. Rong, D. Chu, Journal of Power Sources 126 (2004) 119–124.
[7] D. Chu, R. Jiang, Electrochimica Acta 51 (2006) 5829–5835.
[8] J.G. Liu, T.S. Zhao, Z.X. Liang, R. Chen, Journal of Power Sources 153 (2006) 61–67.
[9] S.H. Seo, C.S. Lee, Applied Energy 87 (2010) 2597–2604.
[10] J.P. Meyersa, J. Newman, Journal of the Electrochemical Society 149 (2002) A718–A728.
[11] Z.H. Wang, C.Y. Wang, Journal of the Electrochemical Society 150 (2003) A508–A519.
[12] G. Murgia, L. Pisani, A.K. Shukla, K. Scott, Journal of the Electrochemical Society 150 (2003) A1231–A1245.
[13] S. Srinivasan, E.A. Ticianelli, C.R. Derouin, A. Redondo, Journal of Power Sources 22 (1988) 359–375.

[14] J. Kim, S.M. Lee, S. Srinivasan, C.E. Chamberlin, Journal of the Electrochemical Society 142 (1995) 2670–2674.
[15] G. Squadrito, G. Maggio, E. Passalacqua, F. Lufrano, A. Patti, Journal of Applied Electrochemistry 29 (1999) 1449–1455.
[16] D. Chu, R. Jiang, Journal of Power Sources 80 (1999) 226–234.
[17] K. Scott, P. Argyropoulos, K. Sundmacher, Journal of Electroanalytical Chemistry 477 (1999) 97–110.
[18] P. Argyropoulos, K. Scott, A.K. Shukla, C. Jackson, Fuel cells 2 (2002) 78–82.
[19] P. Argyropoulos, K. Scott, Journal of Power Sources 123 (2003) 190–199.
[20] H.C. Tu, Y.Y. Wang, C.C. Wan, K.L. Hsueh, Journal of Power Sources 159 (2006) 1105–1114.
[21] B.L. García, V.A. Sethuraman, J.W. Weidner, R.E. White, Journal of Fuel Cell Science and Technology 1 (2004) 43–48.
[22] S. Eccarius, B.L. Garcia, C. Hebling, J.W. Weidner, Journal of Power Sources 179 (2008) 723–733.
[23] A. Casalegno, R. Marchesi, D. Parenti, Fuel Cells 8 (2008) 37–44.
[24] A. Casalegno, R. Marchesi, Journal of Power Sources 185 (2008) 318–330.
[25] Y.J. Chiu, International Journal of Hydrogen Energy 35 (2010) 6418–6430.
[26] Y.J. Chiu, Efficiency optimization subject to various operating variables of a direct liquid-feed fuel cell system, Project report of the National Science Council, Taiwan, R.O.C. (NSC 98-2221-E-149-009), 2010.
[27] R.E. Sonntag, C. Borgnakke, Introduction to Engineering Thermodynamics, John Wiley & Sons, New York, 2001.
[28] E. Springer, T.A. Zawodzinski, S. Gottesfeld, Journal of the Electrochemical Society 138 (1991) 2334–2342.
[29] J.T. Wang, S. Wasmus, R.F. Savinell, Journal of The Electrochemical Society 143 (1996) 1233–1239.
[30] T.Z. Yan, T.C. Jen, International Journal of Heat and Mass Transfer 51 (2008) 1192–1204.
[31] H. Dohle, J. Divisek, J. Mergel, H.F. Oetjen, C. Zingler, D. Stolten, Journal of Power Sources 105 (2002) 274–282.
[32] J.P. Norton, An Introduction to Identification, Academic Press Inc., London, 1986.